

Coherence resonance and ice ages

Jon D. Pelletier

Department of Geosciences, University of Arizona, Tucson, Arizona, USA

Received 31 October 2002; revised 2 July 2003; accepted 21 July 2003; published 28 October 2003.

[1] The processes and feedbacks responsible for the 100-kyr cycle of Late Pleistocene global climate change are still being debated. This paper presents a numerical model that integrates (1) long-wavelength outgoing radiation, (2) the ice-albedo feedback, and (3) lithospheric deflection within the simple conceptual framework of coherence resonance. Coherence resonance is a dynamical process that results in the amplification of internally generated variability at particular periods in a system with bistability and delay feedback. In the Late Pleistocene climate system, bistability results from a combination of long-wavelength outgoing radiation and the ice-albedo feedback. These processes are in equilibrium at interglacial and full-glacial conditions. Delay feedback results from the influence of lithospheric deflection on ice sheet advance and retreat. This process has commonly been represented in numerical climate models by complex models of ice sheet dynamics. As an alternative, the present model incorporates ice sheet dynamics implicitly by using the observed relationship between ice coverage and global temperature. The result is a simple, well-constrained model for the Late Pleistocene global climate system with only one free parameter. The model accurately reproduces the climate variability recorded in the Vostok ice core from timescales of several thousand to one million years, including the histograms and power-spectral behavior of the data. The 100-kyr cycle is a free oscillation in the model, present even in the absence of external forcing. The model also reproduces smaller-amplitude periodicities at odd harmonics of 100 kyr, suggesting that a significant portion of the spectral power at the Milankovitch bands of 41 and 29 kyr may be internally generated. Finally, the development of 100-kyr oscillations in the Mid-Pleistocene may be understood within this model framework as the transition from a climate with one stable state to a system with two stable states brought about by the development of large continental ice sheets and the addition of the ice-albedo feedback to the climate system. *INDEX TERMS*: 3220 Mathematical Geophysics: Nonlinear dynamics; 3344 Meteorology and Atmospheric Dynamics: Paleoclimatology; 3367 Meteorology and Atmospheric Dynamics: Theoretical modeling; *KEYWORDS*: Pleistocene climate, stochastic, energy balance

Citation: Pelletier, J. D., Coherence resonance and ice ages, *J. Geophys. Res.*, 108(D20), 4645, doi:10.1029/2002JD003120, 2003.

1. Introduction

[2] There is widespread agreement that significant periodicities in the time series of Late Pleistocene global climate near 29 and 41 kyr are controlled by the precession and obliquity of Earth's orbit. There is little agreement, however, on which processes and feedbacks control other characteristics of Late Pleistocene climate, including the 100-kyr cycle and the asymmetry of glacial-interglacial transitions. Many models have been introduced over the past few decades that reproduce one or more of these features. Several of the most successful models have focused on nonlinear feedbacks between continental ice sheet growth, radiation balance, and lithospheric deflection [e.g., Oerlemans, 1980a, 1980b; LeTreut and Ghil, 1983; Pollard, 1983; Hyde and Peltier, 1985]. Recent models, however, have also been developed based on biogeochem-

ical cycles [van der Sluijs *et al.*, 1996] and sea-ice processes [Tziperman and Gildor, 2003]. For several reasons, no model has achieved widespread support [Raymo, 1998]. First, although many models have been successful at reproducing one or more important aspects of the climate record, no model has reproduced behavior closely similar to paleoclimatic time series over a wide range of timescales. Second, because there are multiple mechanisms for generating 100-kyr cycles, it is unclear which mechanisms were at work in the Pleistocene climate system by considering published models alone. Third, several classic models have been "abstract," and did not provide specific physical mechanisms for their dynamics [e.g., Saltzman and Sutera, 1984; Paillard, 1998]. Last, because some models have been based on an abundance of free parameters, it is possible that incorrect models were "tuned" to observed behavior. Imbrie and Imbrie [1980] underscored this point by including a complexity "index," the total number of free parameters in the model and input data, in their review of available models. They argued that models with many free

parameters should be viewed with caution because of the likelihood that some of these models may be fit to the observed data even if they do not adequately represent the controlling processes. Models that are tightly constrained by observational constraints and have few free parameters limit this possibility.

[3] Models that include ice sheet dynamics and lithospheric deflection have received particular attention because they often exhibit robust 100-kyr cycles. The coupling of ice sheets and lithospheric deflection provides a characteristic timescale of climate-system response that may resonate with internally or externally generated variability to produce periodic behavior. Despite the success of these models, however, the linkage between specific model processes and characteristics of Late Pleistocene climate has not been firmly established. Several models have included three-dimensional ice sheet geometries, realistic ice-flow laws, and accurate continental geography, while others have modeled the behavior of a single ice sheet in one dimension only. The output from these models has been similarly diverse. *Oerlemans* [1980a], for example, developed a simple one-dimensional ice sheet model with ice flow governed by a nonlinear-diffusion equation, a viscoelastic lithosphere, and periodic forcing of the ice sheet margin. His model reproduced a 100-kyr ice-volume cycle with asymmetric glacial-interglacial transitions similar to those observed. More complex models, however, have not commonly reproduced the rapid deglaciations obtained by *Oerlemans*. *Hyde and Peltier* [1985] and *LeTreut and Ghil* [1983], for example, introduced a more realistic ice sheet rheology and geometry into their models. These improvements resulted in generally sluggish ice sheet retreat inconsistent with the observed record. Most recently, several ice sheet-bedrock models have incorporated mass-wasting processes, such as ice calving [*Pollard*, 1983; *DeBlonde and Peltier*, 1993], and basal-flow enhancements [*Tarasov and Peltier*, 1999] in order to minimize discrepancies between their model output and observed behavior. While these adjustments led to behavior more consistent with observations, they came at the price of increased model complexity and the additional free parameters that prevent a direct, unique linkage between model behavior and observations.

[4] The aim of this paper is to present a model of Late Pleistocene climate that builds upon classic work in ice sheet-bedrock modeling in a way that clearly establishes the controlling processes of ice-age cycles in a simple, easily reproducible model. The model is not meant to replace previous ice sheet-bedrock models but to compliment them and highlight their fundamental processes and feedbacks. The model incorporates the classic mechanisms of ice sheet-bedrock models but is simpler, because temperature is represented by a single, globally averaged variable. The model includes only one free parameter, with the remaining parameters tightly constrained with independent data.

2. Coherence Resonance

[5] The 100-kyr oscillation in the model is reproduced with no external periodic forcing. The model produces output independent of and linearly superimposed on orbital forcing variations. The process at work is coherence resonance. Coherence resonance has been investigated by sta-

tistical physicists for several years [e.g., *Pikovsky and Kurths*, 1997; *Masoller*, 2002]. The necessary components of a coherently resonating system are (1) bistability, (2) delay feedback, and (3) random variability [*Tsimring and Pikovsky*, 2001]. A number of physical, chemical, and biological systems have these components and exhibit coherence resonance [e.g., *Lee et al.*, 1998; *Giacomelli et al.*, 2000; *Liu et al.*, 2002]. A bistable system is one with two stable states. For example, a ball that rolls back and forth between two valleys when pushed over a hill is a bistable system. Random noise may be introduced into this system to produce “kicks” that may push the ball over the hill and into the other valley. Kicks may accumulate over time in a way that is analogous to the Brownian motion of a molecule in a fluid. Normally, the kicks tend to cancel each other out keeping the ball trapped in one valley. From time to time, however, a series of kicks in the same direction will occur that move the ball over the hill. Delay feedback occurs if an additional force is exerted on the ball that is not random, but depends on the elevation of the ball at a previous time.

[6] There are two timescales in this system: the delay time and the average time interval between divide crossings. This latter timescale is controlled by the height of the hill and the magnitude of the random variability. If these two timescales are close in value, a resonance occurs in which the random switching between valleys is made more regular by the delay feedback which encourages a repetition in the history of the system. For example, if a series of random kicks move the ball over the hill, the delay feedback will act to push the ball up over the hill in the same manner at a later time by providing systematic kicks in the uphill direction. This behavior is strongly self-reinforcing: the more regularly a ball makes its way up over the hill, the more regularly will the delay feedback work to systematically push it up the hill at the later time.

[7] The prototypical equation for coherence resonance is

$$\frac{\Delta T_n}{\Delta t} = T_n - T_n^3 + \epsilon T_{n-\tau} + D\eta_n \quad (1)$$

where T is the system variable (e.g., elevation in the case of a rolling ball, or temperature in the climate system), n is the time step, τ is the delay time, and η is a white noise with standard deviation D . The first two terms on the right side of equation (1) represent bistability in the system. The delay feedback and noise are represented by the third and fourth terms, respectively. Systems with both positive and negative feedback may occur depending on whether ϵ is positive or negative. Coherence resonance occurs in both cases, but with a different periodicity.

[8] An example of model output from equation (1) is plotted in Figure 1a, with the corresponding power spectrum plotted in Figure 1b. Model parameters for this example are $\tau = 600$, $\epsilon = -0.1$, and $D = 0.1$. The power spectrum in Figure 1b was computed by averaging the spectra of 1000 independent model time series to reduce the uncertainty in the power-spectral estimation. The time series in Figure 1a has two stable states at $T = +1$ and $T = -1$. The system switches between these states with a period equal to $\tau/2$, despite the absence of any periodic terms in the model equation. In Figure 1, I have illustrated

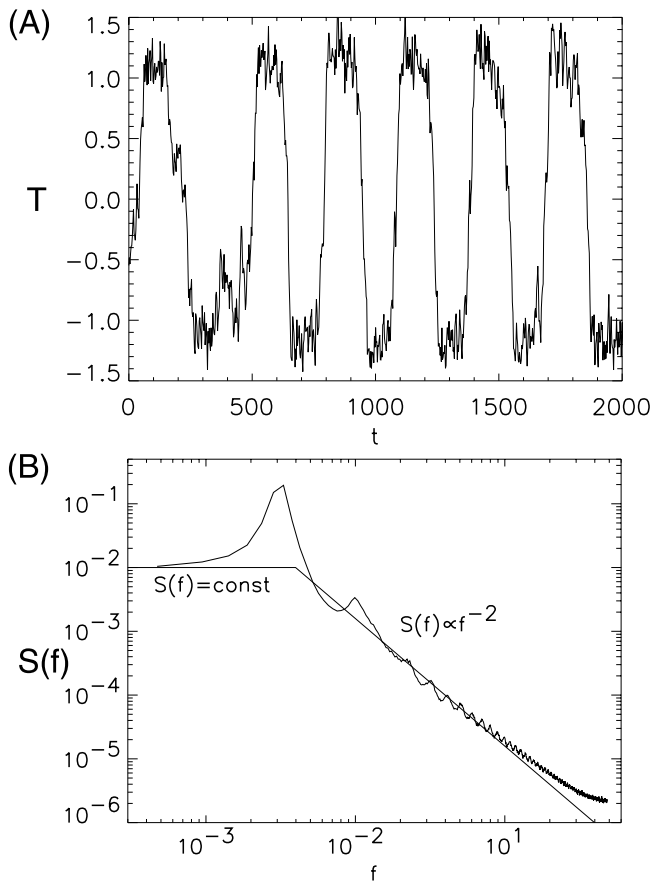


Figure 1. Example of coherence resonance in equation (1). (a) Time series of equation (1) with $\tau = 600$, $\epsilon = -0.1$, and $D = 0.1$. The time series of model output exhibits a cycle with an average period of 300 time steps. (b) Average power spectrum of 1000 samples of the model illustrated in Figure 1a. The power spectrum has a dominant peak with a period of $\tau/2$ and smaller-amplitude periodicities at odd harmonics of the dominant periodicity, superposed on a “background” spectrum that is constant at small frequencies and proportional to f^{-2} at larger frequencies.

the negative feedback case by choosing $\epsilon < 0$. Positive feedback produces a similar output, but with a dominant period equal to τ rather than $\tau/2$ [Tsimring and Pikovsky, 2001]. Less-dominant periodicities also occur at odd harmonics of the dominant periodicity (i.e., periods of $\tau/6$, $\tau/10$, $\tau/14$, etc.) in Figure 1b. The “background” spectrum in Figure 1b is constant for low frequencies and proportional to f^{-2} above a threshold frequency. This is called a Lorentzian spectrum and is a common feature of stochastic models with a restoring or negative feedback. A Lorentzian spectral signature was documented in Late Pleistocene paleoclimatic time series data by Komintz and Piasias [1979], suggesting a stochastic element to the climate system limited by a negative feedback mechanism at long timescales. This observation was the basis for many stochastic climate models, including those of Hasselmann [1971], Nicolis and Nicolis [1984], North et al. [1981], and Pelletier [1997], among others.

[9] Periodic behavior in equation (1) occurs through a resonance between delay feedback and the switching rate.

Without delay feedback, T switches back and forth randomly between the two stable states of the system with an average rate given by Kramer’s formula, a classic equation in statistical physics. For equation (1) this rate is given by

$$R = \frac{1}{\sqrt{2\pi}} \exp\left(\frac{-1}{4\sqrt{2D}}\right) \quad (2)$$

The time interval between transitions in the absence of delay feedback has a Gaussian distribution with a large variance [van Kampen, 2001]. If the delay feedback is present, however, it works constructively with the internal variability to amplify the system response at the delay timescale. The result is a distribution of switching times that becomes progressively narrower as the feedback term is strengthened.

[10] Coherence resonance should be distinguished from the more commonly known process of stochastic resonance. Stochastic resonance is the basis for models of Pleistocene climate proposed by Nicolis and Nicolis [1984] and Matteucci [1990], as well as more recent models of Dansgaard-Oeschger events by Ganopolski and Rahmsdorf [2001]. Stochastic resonance works when an external periodic force is applied to a bistable system with noise. The noise is amplified by the external periodic force to create a periodic response with a period equal to that of the external forcing. Stochastic resonance may have applications to the Pleistocene climate system. However, as it was originally proposed, stochastic resonance predicts symmetric glacial and interglacial states [Matteucci, 1989]. Therefore stochastic resonance is inconsistent with the observed dominance of glacial climates in the Late Pleistocene and the asymmetry of glacial-interglacial transitions.

[11] The climate model of this paper is a single finite difference equation for global temperature analogous to equation (1). Bistability in the model is based on a balance between the negative feedback of long-wavelength outgoing radiation and the positive ice-albedo feedback. The negative feedback of outgoing radiation is dominant in an Earth without extensive subpolar ice sheets. When large continental ice sheets expand in North America and Northern Europe, however, temperature drops result in an albedo increase large enough to dominate the negative feedback of outgoing radiation. The net positive feedback driven by ice sheet expansion sends the climate system into a self-enhancing feedback of colder temperatures and larger ice sheets. This feedback, however, continues only as long as ice sheets expand nonlinearly with global temperature, however. The fact that ice sheets grow preferentially on the continents eventually weakens the positive feedback as the North American ice sheets expand into a tapering continent. The result is a second stable climate state characterized by an equilibrium between the ice-albedo feedback and the negative feedback of outgoing radiation.

3. Model Processes

3.1. Long-Wavelength Outgoing Radiation

[12] The Earth maintains a mean global temperature of approximately 15°C through a balance between incoming solar radiation and long-wavelength outgoing radiation. Long-wavelength outgoing radiation is characterized by

the Stefan-Boltzmann Law, in which outgoing radiated energy depends on the fourth power of absolute temperature. For small temperature fluctuations around an equilibrium temperature, the T^4 Boltzmann dependence may be linearized to yield the finite difference equation [North *et al.*, 1981]

$$C \frac{\Delta T_n}{\Delta t} = -BT_n \quad (3)$$

where n is an index of the time step, C is the heat capacity per unit surface area of the atmosphere-ocean-cryosphere system, B is the coefficient of temperature dependence of outgoing radiation, and T_n is the temperature difference from equilibrium. This equation characterizes a negative feedback: global warming (cooling) resulting from short-term climatic fluctuations results in more (less) outgoing radiation. C may be estimated from the specific heat of water, $4.2 \times 10^3 \text{ J/kg/}^\circ\text{C}$, and the mass of the oceans, $1.4 \times 10^{21} \text{ kg}$, and the surface area of the Earth, $5.1 \times 10^{14} \text{ m}^2$, to obtain $C = 1.2 \times 10^{10} \text{ J/}^\circ\text{C}$, assuming that the heat capacity of the climate system is dominated by the oceans. The value of B is constrained from satellite measurements to be $2.1 \text{ J/s/m}^2/^\circ\text{C}$ [Short *et al.*, 1984; North, 1991]. The ratio of B to C is defined to be c_1 in this paper and defines a radiative-damping timescale for the climate system equal to 180 yr (the inverse of c_1). (The simple linear relationship between temperature change and mean global temperature in equation (3) is plotted in Figure 3a.)

[13] The negative feedback of equation (3) is balanced by natural variability in Earth's radiation balance driven by short-term (decadal and centennial) fluctuations in atmospheric temperature. These fluctuations create random variability in long-wavelength outgoing radiation. This variability may be modeled by introducing a random noise in equation (3) to obtain [Hasselmann, 1971; North *et al.*, 1981]

$$\frac{\Delta T_n}{\Delta t} = -c_1 T_n + D\eta_n \quad (4)$$

where η is a white noise with standard deviation equal to D . Short-term internal temperature variations generate significant low-frequency temperature variations because the climate system integrates the short-term random variations through their effect on the outgoing radiation flux. The result of this process is Brownian-walk behavior for global temperature. Equation (4) has the behavior of a damped Brownian walk, however, because the equation also includes a negative feedback term.

3.2. Ice-Albedo Feedback

[14] The growth of ice sheets provides a positive feedback that dominates the negative feedback of outgoing radiation if ice sheets grow nonlinearly with global temperature. The effects of the ice-albedo feedback on global climate may be modeled by including a term in equation (3), $a(T)$, which reflects the dependence of Earth's albedo on global temperature, to obtain

$$\frac{\Delta T_n}{\Delta t} = -c_1 T_n - c_2 a(T_n) \quad (5)$$

I assume that the modern interglacial state is a steady state of the climate system. This provides the constraint $a(0) = 0$ and fixes the temperature of any other stable states of the system to be with respect to an origin at the modern interglacial temperature.

[15] Stable states or fixed points of equation (5) are determined by setting the right side equal to zero. $T = 0$, the modern interglacial, is a fixed point because I defined $a(0) = 0$. Whether or not another fixed point exists depends on how $a(T)$ increases with decreasing T . If the Earth's albedo increases greater than linearly with T , the positive ice-albedo feedback dominates the system. A dominant ice-albedo feedback leads to an ice-covered Earth if $a(T)$ increases greater than linearly for all T . However, if the ice-albedo feedback increases less than linearly for any T , the combination of outgoing radiation and the ice-albedo feedback will be negative or self-limiting for those values of T .

[16] Determining the form of $a(T)$ is complicated by uncertainties in the geographic distribution of ice as a function of global temperature. Most numerical ice sheet-climate models determine $a(T)$ by ice sheet dynamics in their full complexity, including internal flow, basal sliding, and mass wasting. The complexity of these models results in dozens of free parameters for the motion of continental ice sheets. These processes, especially basal sliding, are poorly constrained. The distribution of sea ice as a function of global temperature is also highly uncertain.

[17] As an alternative to modeling ice sheet dynamics, the extent of land ice through time during the last deglaciation may be inferred from the pattern of postglacial rebound [Peltier, 1994]. Peltier's reconstruction provides ice extents at 1-kyr intervals from the Last Glacial Maximum (LGM) to the present. His reconstruction provides data on ice sheet topography as well as extent, but only the data on ice sheet extent are necessary to constrain variations in albedo. I estimated the relationship between global albedo and temperature from the LGM to the present using Peltier's ice extents and the Vostok time series. First, a global temperature time series was constructed by averaging the Vostok time series in 1-kyr intervals centered on each integer value of kyr. At timescales of millenia, paleoclimatic data from the Northern and Southern Hemispheres are strongly correlated [e.g., Bender *et al.*, 1994]. This observation provides a basis for using Vostok data to represent a global-average temperature at these timescales. The time-averaged Vostok data provide the independent data to determine $a(T)$. The dependent data were obtained by multiplying each $1^\circ \times 1^\circ$ grid square in Peltier's data by its area and the amount of incident solar radiation it receives to obtain the relative change in albedo as a function of global temperature:

$$a(T) = \sum_{i=-180}^{180} \sum_{j=-90}^{90} a_{i,j}(T) \cos^2(j) \quad (6)$$

where $a_{i,j} = 0.25$ if the grid square is ice-free and $a_{i,j} = 0.85$ if the grid square is ice-covered.

[18] Equation (6) provides an estimate of the relative change in Earth's albedo due to the presence of Late Pleistocene continental ice sheets. The albedo difference between modern and LGM conditions calculated in equation (6) equals 10% of the modern albedo assuming that ice-free

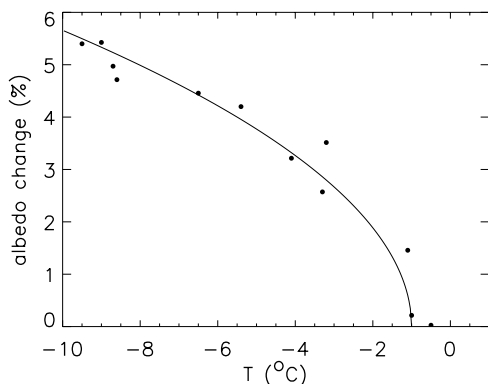


Figure 2. Observed relationship between albedo and global temperature based on *Peltier's* [1994] gravitationally self-consistent sea level inversion and Vostok temperatures for the same time periods. The data closely approximate a square-root function between albedo and global temperature ($a(T) = c_2(T_h - T)^{\frac{1}{2}}$ with $T_h = -1$). The shape of this curve largely reflects the sensitivity of the Laurentide ice sheet coverage to global temperatures as the ice sheet retreated westward and southward from Hudson Bay during late stage of retreat. Earlier stages of retreat were not as sensitive because ablation resulted in limited retreat due to the tapered ice sheet geometry in southern Canada.

areas are also continuously snow free as well. 10% is an overestimate, however, because many areas assumed to be ice-free in equation (6) have seasonal snow and ice cover. Accounting for modern seasonal snow and sea-ice cover, *Oerlemans* [1980a] estimated that the albedo difference between the LGM and the present was approximately 5%. I have used this value to scale the albedo curve to a maximum change of 5% between the present and the LGM. In other words, I have used *Oerlemans'* albedo estimate for the total change between the LGM and the present, and *Peltier's* reconstructions to estimate the relative change through time. The result is plotted in Figure 2. It should be emphasized that this approach does not include the effects of changes in sea-ice coverage between the LGM and today, which are not well constrained.

[19] The data of Figure 2 are well approximated by a square-root function:

$$a(T) = \begin{cases} (T_h - T)^{\frac{1}{2}} & \text{if } T < T_h \\ 0 & \text{if } T \geq T_h \end{cases} \quad (7)$$

where $T_h = -1^\circ\text{C}$ (relative to the modern temperature) is the temperature at which subpolar ice sheet growth is initiated in Hudson Bay. The value of the coefficient of $a(T)$, c_2 , is given by

$$c_2 = \frac{Q a(T_g) - a(T_h)}{C (T_h - T_g)^{\frac{1}{2}}} \quad (8)$$

where T_g is the temperature of the full glacial climate state, Q , the incoming solar energy, is equal to 340 J/s/m^2 [*North*, 1991]. Equation (8) yields $c_2 = 5.4 \times 10^{-10} \text{ }^\circ\text{C}^{\frac{1}{2}}/\text{s}$. Scaled to the radiative timescale of 180 yr this is $c_2 = 3.0^\circ\text{C}^{\frac{1}{2}}$. The relationship between incoming energy and

global temperature is plotted in Figure 3b. The combination of the ice-albedo feedback and long-wavelength outgoing radiation are illustrated in Figure 3c. The combined effect of these processes results in two fixed points in the model system corresponding to the full glacial and interglacial states.

[20] I assume that equation (7) holds for both glaciations and deglaciations throughout the Late Pleistocene if the lithosphere is held fixed. This assumption implies that ice sheet extents depend only on the instantaneous global temperature and not on whether temperature is increasing or decreasing. The influence of lithospheric deflection on ice sheet advance and retreat will be characterized with a separate term in the model equation, providing the mechanism for the asymmetry between glaciations and deglaciations.

[21] The square-root function of equation (7) masks a great deal of complexity, including both the topography and shape of the continents of the polar and subpolar regions. The square-root form may be approximately understood by

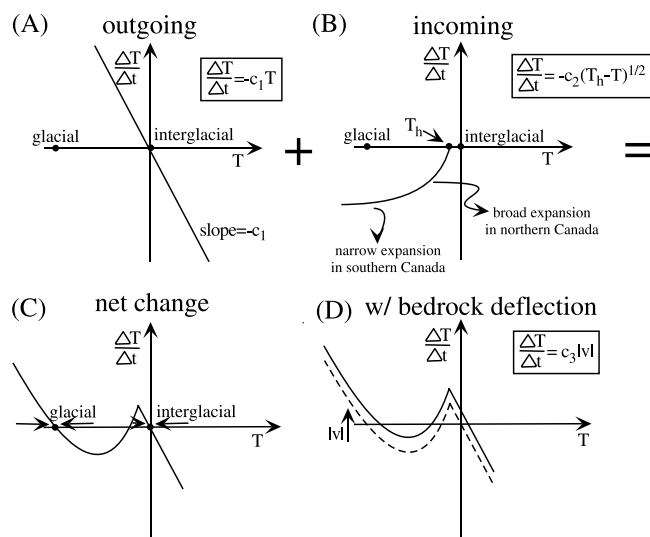


Figure 3. Schematic diagram of processes included in our radiation-balance model. Each graph is a sketch of the functional relationship between temperature change, $\Delta T/\Delta t$, and global temperature, T , for each process. (a) A high global temperature results in more outgoing long-wavelength radiation (and relative cooling). This effect is proportional to the temperature difference from equilibrium where the constant of proportionality, c_1 , is equal to the radiation damping time, constrained to be $c_1 = 180 \text{ yr}$ as described in the text. (b) Lower global temperatures result in increased albedo (and relative cooling) with a function that depends on the ice sheet distribution in Figure 2. (c) Long-wavelength outgoing radiation and the ice-albedo feedback taken together yield a system with two fixed points, corresponding to glacial and interglacial states. (d) Bedrock subsidence and rebound modify the effects of the ice-albedo feedback by shifting the curve toward greater relative warming by an amount proportional to $|v|$. Figure 5 illustrates this effect by decomposing ice sheet motion into accumulation-ablation and viscoelastic components of advance and retreat.

considering the constraints on the North American ice sheets (including the Laurentide and former ice sheets) as they expand from their initial location in Hudson Bay. When the North American ice sheet is expanding southward and westward across Canada during its initial growth, the Earth's albedo is sensitive to small changes in global temperature. The result is a strong positive feedback between cooler temperatures and larger ice sheets. The ice sheet eventually reaches its maximum westward extent in northern Canada as the global temperature further drops, however. If ice sheets expand preferentially on land, the ice-albedo feedback weakens at this stage because a further decrease in global temperature results in smaller changes in ice sheet extent because expansion is limited to a southerly direction and a tapering North America. The combined effect of long-wavelength outgoing radiation and the ice-albedo feedback is positive and of large magnitude for small ice sheets, but becomes progressively weaker as ice sheets grow in extent and are eventually geographically limited in where they can expand. As global temperature continues to drop, a balance is eventually achieved between the long-wavelength outgoing radiation and the increase in Earth's albedo. This is the full-glacial climate.

3.3. Fixed Points of the Model Climate System

[22] Figure 3c illustrates the radiation balance of the Earth as a function of global temperature for the combination of long-wavelength outgoing radiation and the ice-albedo feedback. The fixed points are obtained by setting equation (8) equal to zero to obtain

$$T = c_2(-1 - T)^{\frac{1}{2}} \quad (9)$$

with $c_2 = 3.0^\circ\text{C}^{\frac{1}{2}}$. This quadratic equation has two roots at $T = -1.1$ and $T = -8.0^\circ\text{C}$. The root at $T = -8.0^\circ\text{C}$ is a stable fixed point; cooling below this point leads to a net warming and a return to the fixed point. The root at $T = -1.1^\circ\text{C}$ is an unstable fixed point. Equation (8) predicts two stable states of the Late Pleistocene climate system: an interglacial climate with $T = 0^\circ\text{C}$ and a full-glacial climate with $T = -8^\circ\text{C}$. This analysis is independent of the system dynamics and depends only on equilibria of equation (5). The agreement between this prediction and the observed record provides strong evidence that a balance between outgoing radiation and the ice-albedo feedback define the stable states of the Late Pleistocene climate system.

[23] The existence of two stable states is a robust feature of the model. The temperature difference between the predicted glacial and interglacial states depends sensitively on the value of c_2 . However, as long as the ice-albedo feedback declines in strength with decreasing global temperature, a second stable climate state exists for a broad range of model parameters. Whether or not the ice-albedo feedback actually decreases depends most strongly on the relative distribution of land and sea ice. In the simplest model of a snowball Earth, for example, radially symmetric polar ice sheets generate a runaway ice-albedo feedback [North, 1991]. If ice sheets expand preferentially on land, however, the ice-albedo feedback is not a runaway process. The preferential expansion of ice sheets on land and the existence of a stable climate state within the model framework of equation (5) is consistent with CLIMAP

reconstructions of the LGM which place land ice as far south as 40°N while freezing sea-surface temperatures extended only as far south as 60°N latitude in the Northern Hemisphere.

3.4. Lithospheric Deflection

[24] The flexural-isostatic deflection of the lithosphere beneath an ice sheet may have at least two effects on the geometry of the ice sheet. First, lithospheric subsidence may lower accumulation rates by decreasing the ice sheet elevation. This "load-accumulation" feedback is perhaps the most well-studied effect of lithospheric deflection on climate [North, 1991]. The strength of this feedback, however, is limited by another effect of lithospheric subsidence: changes in lateral ice-flow velocities. An ice sheet may be considered to be a conveyor belt in which ice flows from zones of accumulation to zones of ablation. In steady state, this flow occurs without a change in surface topography or ice thickness. In fact, an increase in accumulation may be completely accommodated by an increase in lateral ice-flow velocities such that no change in ice volume occurs. This possibility highlights the difficulty of modeling ice sheet response to the small changes in insolation experienced during the Pleistocene. In particular, a small change in basal-sliding parameters may greatly change the sensitivity of ice sheets to external forcing. Basal-sliding parameters are poorly known, introducing great uncertainty into forward models of climate based on ice sheet dynamics.

[25] Although the absolute values of basal-sliding parameters are poorly known, the relative effects of lithospheric deflection on ice sheet sliding may be determined more precisely. Lithospheric subsidence perturbs a steady state ice sheet by increasing the basal slope of the ice sheet, reducing the gravitational force available to drive lateral ice flow. This flow reduction thickens the ice even under conditions of uniform mass balance. Conversely, lithospheric rebound enhances lateral ice-flow velocities and results in ice sheet thinning.

[26] The effects of lithospheric subsidence and rebound may be illustrated by considering the steady state geometry of an ice sheet sliding on its bed. Ice sheet reconstructions and forward models of ice sheet dynamics suggest that basal sliding was the dominant component of motion in Pleistocene ice sheets [Tarasov and Peltier, 1999]. The geometry of a sliding ice sheet may be determined using an analogy with an ideal-plastic ice sheet. The ideal-plastic model assumes that ice sheet motion is accommodated by internal deformation within a very thin basal layer when the basal shear stress exceeds the yield stress of ice. This is closely analogous to the case of an ice sheet sliding on its bed, in which sliding occurs when the shear stress is greater than the threshold coefficient of sliding friction. This analogy implies that all of the equations derived for an ideal-plastic ice sheet may be applied to the case of a sliding ice sheet by replacing the yield stress with the coefficient of sliding friction. For example, Nye [1951] determined the steady state ice sheet thickness, h , of an ideal-plastic ice sheet on a flat surface to be determined by

$$h = \sqrt{2h_0(L - x)} \quad (10)$$

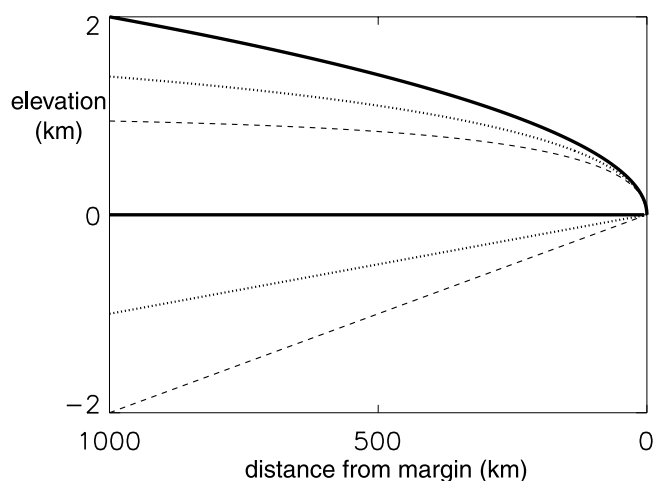


Figure 4. Steady state ice-surface profiles of a plastic ice sheet with different scenarios of bedrock topography, calculated from equations (3) and (4). The elevation of the ice surface and bedrock topography are shown for flat bedrock (solid line), uniformly sloping bedrock (dipping away from the margin) with a slope of $\alpha = 0.002$ (small-dashed line), and $\alpha = 0.004$ (long-dashed line). As the bedrock depression deepens, the ice surface elevation decreases, but not as much as the bedrock. The result is a counterflow within the ice sheet that causes thickening or thinning of the ice sheet depending on whether the lithosphere is subsiding or rebounding.

and the thickness for an ice sheet on a sloping base of gradient α to be

$$x - L = \frac{h}{\alpha} + \frac{h_o}{\alpha^2} \ln|\alpha h - h_o| \quad (11)$$

where L is the length of the ice sheet and h_o is the maximum thickness of the ice sheet on a flat surface. h_o is a function of the sliding shear stress if a sliding rather than a plastic ice sheet is assumed. To illustrate the effects of lithospheric deflection on the ice sheet thickness, I have plotted ice sheet profiles from equation (10) and equation (11) for a flat surface and for surfaces with $\alpha = 0.002$ and 0.004 in Figure 4. These profiles illustrate that as the lithosphere subsides, an ice sheet will thicken because lateral ice flow is inhibited by the increase in basal slope. Conversely, lithospheric rebound leads to ice sheet thinning.

[27] Ice sheet thickening and thinning, in turn, modify the effects of changes in global temperature to retard glaciations and accelerate deglaciations. This coupling may be called the “load-advance” feedback and is illustrated in Figure 5. In Figure 5a, cases 1–3 illustrate how a decrease in lateral ice-flow velocities results in a reduced rate of ice sheet advance. Conversely, in Figure 5b, cases 1–3 illustrate how ice sheet retreat is enhanced by an increase in lateral flow driven by lithospheric rebound. In both cases, lithospheric adjustment acts to increase the albedo relative to cases with a fixed lithosphere. Figure 5a, case 1 illustrates the effect of subsidence on ice sheet geometry: a reduction in lateral ice-flow velocities results in ice sheet thickening as shown in Figure 4. In Figure 5a, case 2, the effects of accumulation

growth are shown in the absence of subsidence. Accumulation is assumed to occur uniformly along the ice sheet profile. The effects of subsidence-induced thickening and accumulation growth taken together are illustrated in Figure 5a, case 3. The combination results in a smaller ice sheet advance relative to the case with accumulation alone. In cases in which accumulation is not uniform (i.e., accumulation increases with distance from the margin) the limiting effect of subsidence on ice sheet advance is even greater. Cases 1–3 in Figure 5b illustrate the load-advance feedback during deglaciation. Case 1 in Figure 5b illustrates lithospheric rebound and resultant ice sheet thinning. Case 2 in Figure 5b illustrates the ice sheet retreat resulting from ablation. Finally, the combination of thinning and ablation is

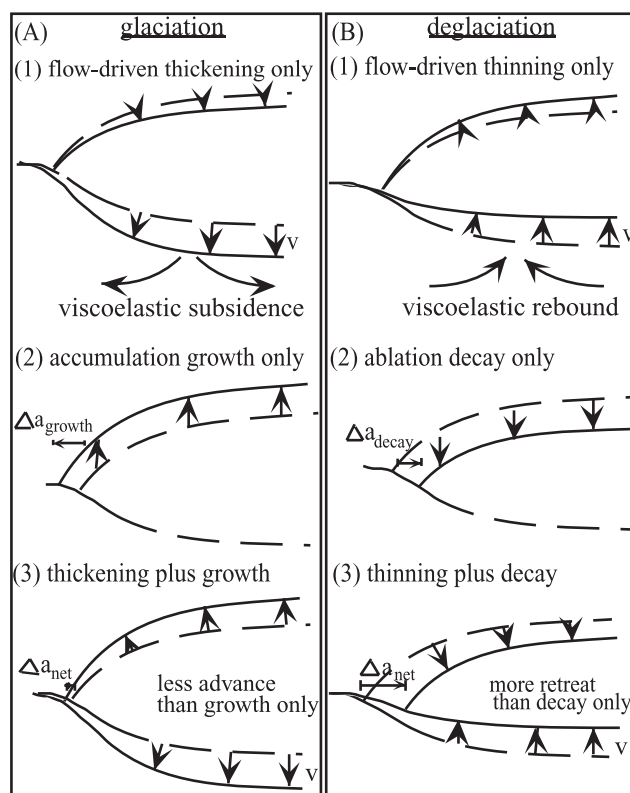


Figure 5. Schematic illustration of the coupling between ice sheet adjustment by lithospheric deflection and ice sheet advance or retreat. The initial bedrock and ice sheet geometry is shown (dashed line) along with the final geometry (solid line) in each case. (a) During glaciation: Bedrock subsidence considered alone leads to ice sheet thickening (case 1). Accumulation growth considered alone leads to uniform thickening (assuming uniform accumulation rate along the ice sheet) with a corresponding advance (case 2). Both processes taken together act destructively because some accumulation growth is cancelled out by subsidence, reducing the effective albedo change (case 3). (b) During deglaciation: Bedrock rebound alone leads to ice sheet thinning (case 1). Ablation alone leads to uniform thinning of the ice sheet with a corresponding retreat (case 2). Together these processes act constructively to modify albedo because ablation results in a greater retreat for a thinner ice sheet (case 3).

shown in Figure 5b, case 3. This figure illustrates how ice sheet thinning enhances retreat.

[28] The effects of lithospheric subsidence and rebound on the motion of an ice margin is dependent on the velocity of the lithosphere, $|v|$, not on its elevation. This is a key difference between the load-accumulation feedback and the load-advance feedback. In the load-advance feedback, the retarding and amplifying effects of case 3 in Figures 5a and 5b are observed only when the lithosphere is actively subsiding or rebounding. With the load-accumulation feedback, in contrast, the reduction in accumulation rate that accompanies subsidence is a function of the bedrock elevation, not its velocity. This is an important distinction, because asymmetric glacial-interglacial transitions are only reproduced in a model with velocity-dependent feedbacks.

[29] To model the load-advance feedback, I have included a term in the model equation (5) proportional to the magnitude of the velocity, $|v|$, given by

$$v_n = \frac{\Delta B_n}{\Delta t} \quad (12)$$

where

$$B_n = \sum_{n'=0}^{n'=n} \frac{T_h - T}{\tau} e^{-(n-n')/\tau} \quad (13)$$

and τ is the Maxwell-relaxation time of the viscoelastic crust [Watts, 2001] and B is the bedrock depth.

4. Model Behavior and Comparison to Vostok Ice Core

[30] The model equation, including long-wavelength outgoing radiation, the ice-albedo feedback, and lithospheric deflection, is

$$\frac{\Delta T_n}{\Delta t} = -c_1 T_n + c_2 (T_h - T_n)^{\frac{1}{2}} + c_3 |v|_n + c_4 \eta_n \quad (14)$$

[31] To simplify, I rescaled equation (14) to make $c_1 = 1$:

$$\frac{\Delta T_n}{\Delta t} = -T_n + c_2 (T_h - T_n)^{\frac{1}{2}} + c_3 |v|_n + c_4 \eta_n \quad (15)$$

[32] Model time steps are equal to the radiative-damping time of 180 yr in equation (15). Equation (15) is analogous to the coherence resonance equation (1). The first two terms on the right side of equation (15) represent the bistability in the system. The third and fourth terms represent the delay feedback and random variability, respectively. The values of c_1 through c_4 and τ used in the reference model run of equation (15) are given in Table 1. The values of c_1 and c_2 have been determined from empirical data in the preceding sections. The value of c_4 may be constrained using the

Table 1. Values of the Parameters in the Reference Model

	c_1, s^{-1}	$c_2, ^\circ C^{\frac{1}{2}}/s$	c_3	$c_4, ^\circ C/s$	τ, kyr
Original	1.8×10^{-10}	5.4×10^{-10}	N/A	N/A	10
Scaled to c_1	1	3.0	25.0	0.9	56

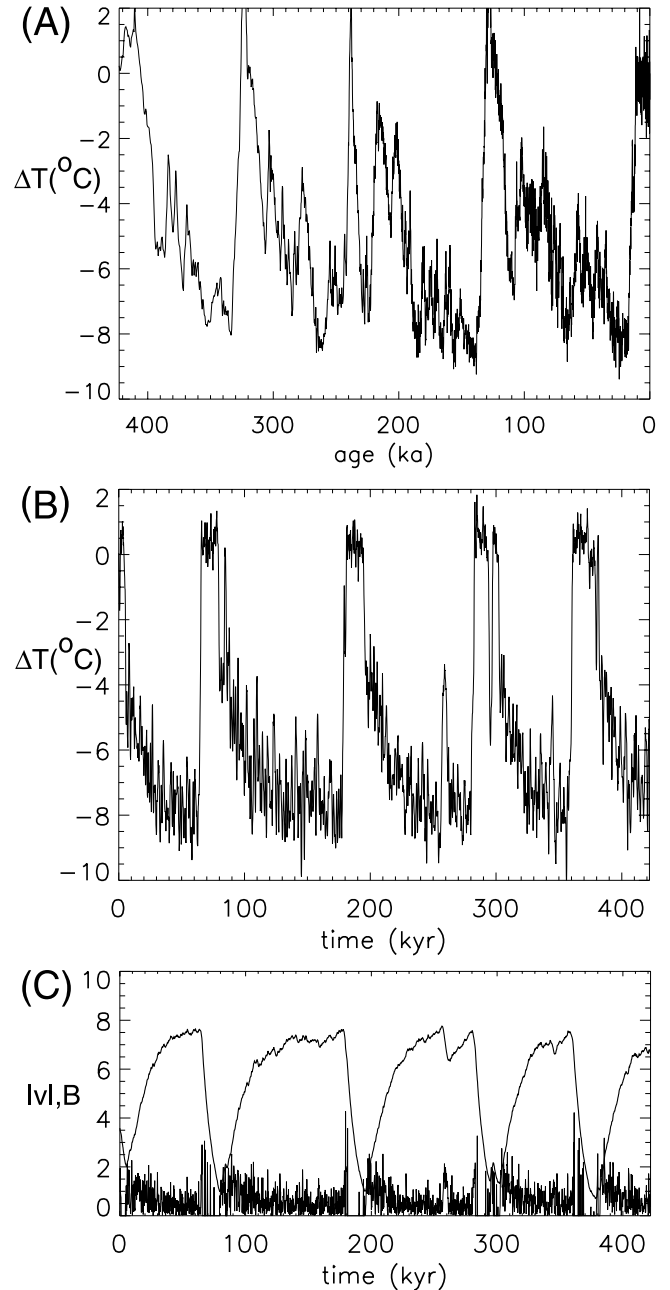


Figure 6. (a) Time series of atmospheric temperature variations inferred from Deuterium concentrations at Vostok, Antarctica [Petit et al., 1999]. (b) Time series of model temperature variations (from equation (15)) with $c_2 = 3.0$, $c_3 = 25.0$, $c_4 = 0.9$, and $\tau = 10$ kyr. (c) Time series of bedrock elevation and velocity in the model example of Figure 6b.

Vostok time series. To do this, I first averaged the Vostok time series in equal intervals of the model scaling time of 180 years. Second, I computed the standard deviation of ΔT_n from the Vostok data. The result is $c_4 = 0.9^{\circ}C$ and quantifies the magnitude of short-term global temperature changes. This value is consistent with other available estimates of natural century-scale global temperature variations. The Maxwell relaxation time of the mantle was chosen to be 10 kyr, a value consistent with postglacial

rebound. The viscous response time of the mantle actually varies with the size of the load so a constant value will only be an approximation. The remaining model coefficient, c_3 , is the only free parameter in the model. This coefficient characterizes the strength of the load-advance feedback, which depends on the geometries and sliding rates of the ice sheets. I have not attempted to constrain this parameter with empirical data because of the complexity of the processes involved. Instead, the model was run with a range of parameters to qualitatively identify the system behavior. Coherence resonance occurs over a broad range of values for c_3 . $c_3 = 25$ was chosen as the reference parameter value for the numerical model experiments because it leads to both coherence resonance and behavior similar to the Vostok time series, including asymmetric transitions.

[33] The behavior of equation (15) is illustrated in Figure 6b with the reference values of Table 1. Variations in bedrock depth B and the magnitude of bedrock velocity $|v|$ are shown in Figure 6c for this run. The Vostok time series is plotted in Figure 6a for comparison. Note that the Vostok data is plotted here with time, not age, increasing toward the right in order to simplify comparison with the model time series.

[34] The model time series reproduces behavior very similar to the Vostok data, including the same temperature range (with full glacial climates 8°C cooler than interglacials), a 100-kyr periodicity, and asymmetric glacial-interglacial transitions. More specifically, glaciations in both the model and observed data are relatively rapid at first but slow prior to a very rapid deglaciation. This pattern may be understood in terms of the strength of radiation feedbacks and the variations in bedrock velocity through time. Glaciations begin rapidly at first, reflecting the strength of the ice-albedo feedback in this early stage. The glaciation slows as it proceeds, reflecting a decrease in the ice-albedo feedback that limits ice advance. Deglaciation is triggered by a warming trend that is long enough to initiate lithospheric

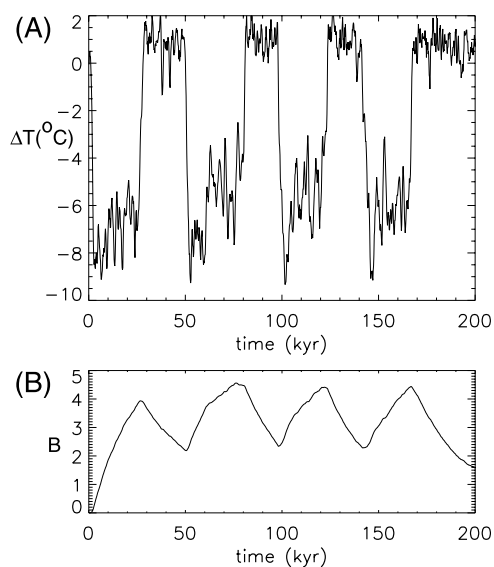


Figure 7. Illustration of model output with delayed feedback coupling to bedrock depth, B , rather than bedrock velocity $|v|$. Time series of (a) global temperature and (b) bedrock deflection are plotted.

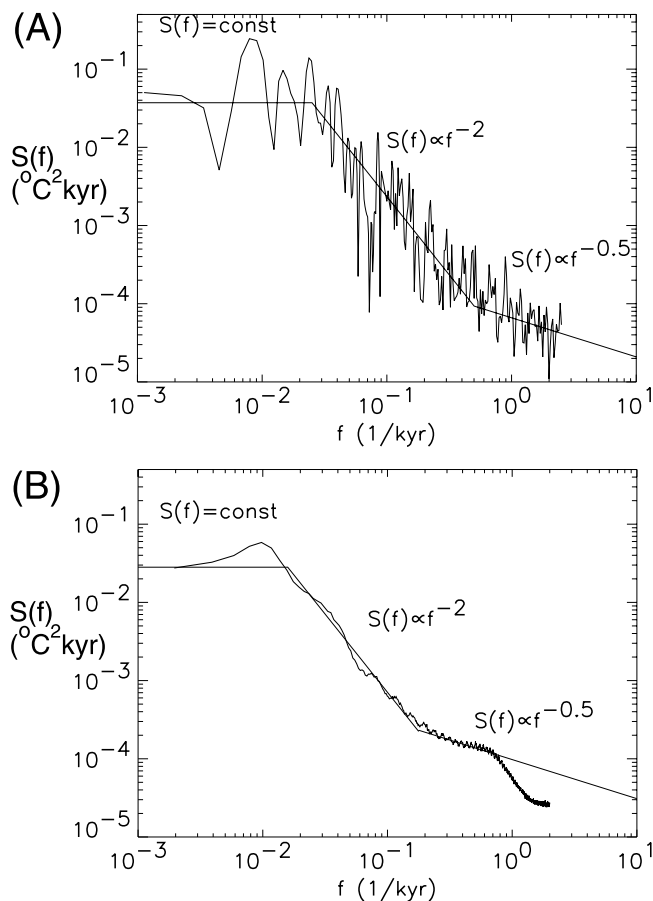


Figure 8. (a) Lomb periodogram, $S(f)$, of Vostok time series data plotted as a function of frequency f . Note logarithmic scales on both axes. Spectrum has a dominant frequency corresponding to a period near 100 kyr, a constant background power spectrum between timescales of 1 Ma and 40 kyr, an f^{-2} spectrum between 40 kyr and 2 kyr, and an $f^{-0.5}$ spectrum at higher frequencies. (b) Average power spectrum of 1000 samples of the model time series illustrated in Figure 6b, with same scale as Figure 8a. The spectrum has a dominant periodicity at 120 kyr superimposed on a background spectrum similar to Figure 8a (except at the highest frequencies). In addition, small-amplitude periodicities appear above the background at odd harmonics of the dominant periodicity.

rebound. The length of the warming trend is important because lithospheric motion lags behind ice loading. Therefore a sustained warming trend is required to initiate deglaciation through the combined effects of ice sheet melting and a lithospheric rebound. During deglaciation, the rebounding lithosphere acts to thin the ice sheet and amplify the ice-albedo feedback in an additional feedback mechanism. In this additional mechanism, faster ice sheet melting results in faster lithospheric rebound and an enhanced ice-albedo feedback. The ice-albedo feedback, in turn, drives rapid ice sheet melting in a positive feedback. It should be noted that even though the relaxation time of the mantle is 10 kyr, the dominant oscillation is close to 100 kyr.

[35] For comparison, I have also investigated the effects of the load-accumulation feedback with a version of equa-

tion (15) that couples $\Delta T_n/\Delta t$ with B instead of $|v|$. In the load-accumulation feedback, ice sheet advance is slowed when the ice sheet elevation is reduced. The load-accumulation effect is proportional to the bedrock depth B rather than its velocity $|v|$. The time series resulting from (14) with $|v|$ replaced by B is given in Figure 7. Coherence resonance occurs in this case to produce periodic behavior. However, in Figure 7, glaciations are more rapid than deglaciations, inconsistent with the climate record. This model result is consistent with models incorporating the load-accumulation feedback that reproduce sluggish deglaciations [e.g., *Le Treut and Ghil, 1983; Hyde and Peltier, 1985*]. These results suggest that the load-advance feedback is the feedback at work in the Pleistocene climate system and that it is responsible for the asymmetry of glacial-interglacial transitions.

[36] The similarity between the model behavior and the Vostok time series may be documented more thoroughly by comparing the histograms and power spectra of both data sets. The power spectra of the Vostok and model time series

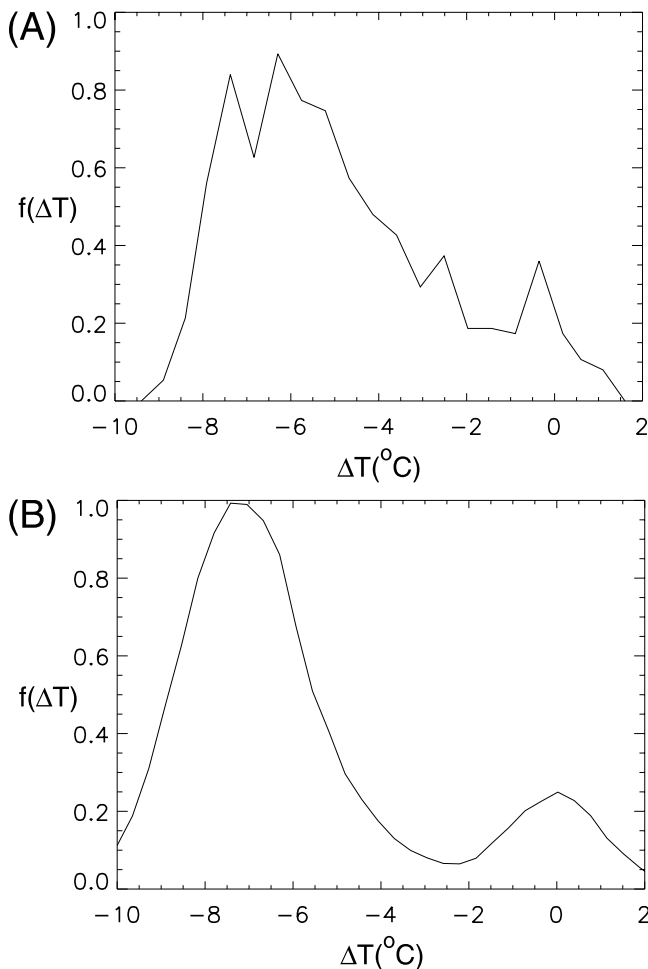


Figure 9. Histograms of (a) Vostok time series data, uniformly sampled at 200 yr intervals, and (b) model time series. These curves reflect the fraction of time the climate is in the interglacial state, the glacial state, or fluctuating in between. The time spent near the glacial state exceeds the time spent near the interglacial state by a fraction of about 5:1.

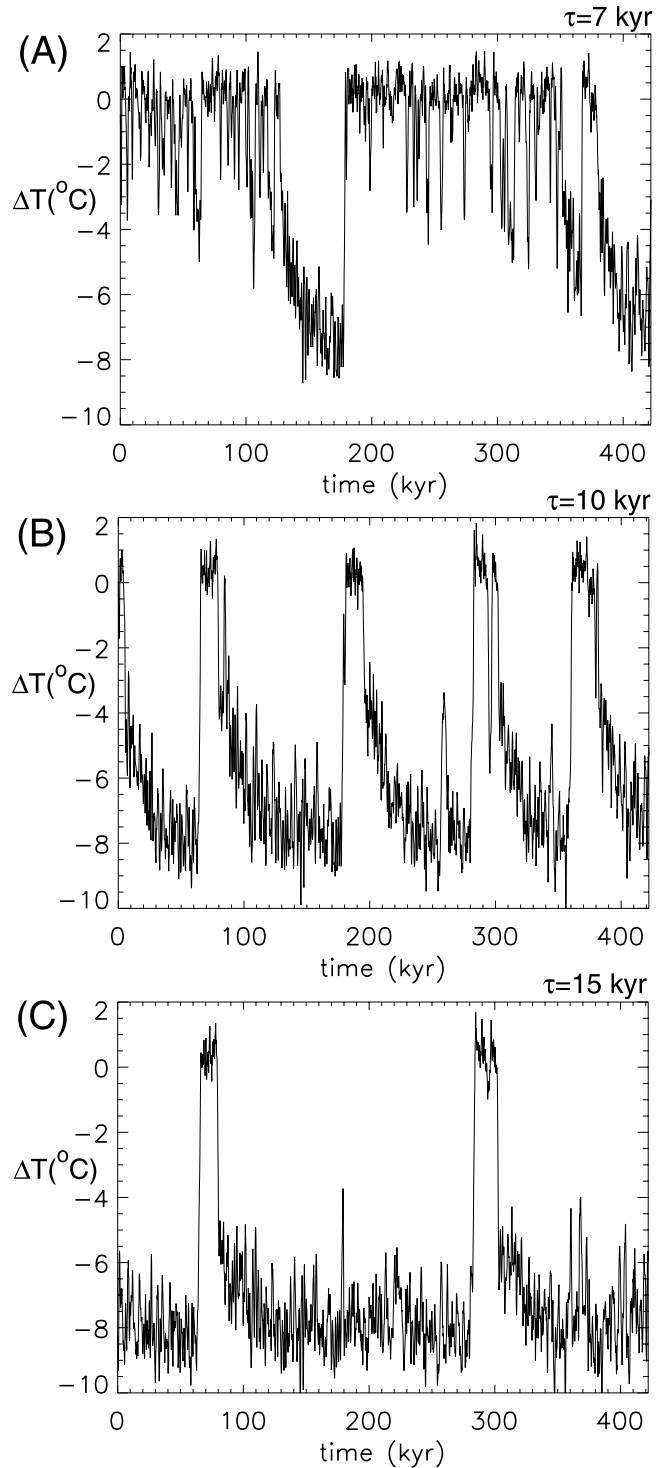


Figure 10. Effects of varying the Maxwell relaxation time, τ , on model behavior. (a) $\tau = 7$ kyr, (b) $\tau = 10$ kyr, and (c) $\tau = 15$ kyr.

are plotted in Figures 8a and 8b, respectively. I estimated the power spectrum of the Vostok time series using the Lomb Periodogram [*Press et al., 1992*]. This technique is commonly used for nonuniformly sampled time series data. The power spectrum of the model time series was estimated by averaging the spectra of 1000 independent samples to obtain a precise spectrum. Both spectra exhibit a dominant

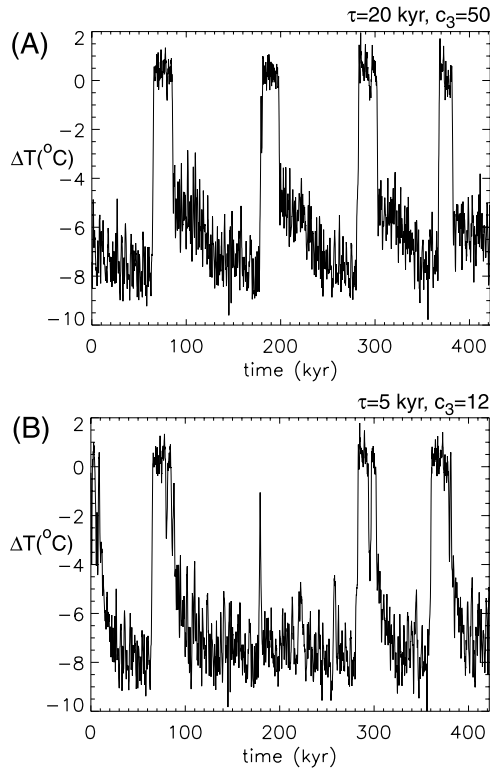


Figure 11. Effects of varying τ and c_3 simultaneously. Time series produced when the values of τ and c_3 are (a) doubled and (b) halved from the reference values of Figure 6b. Resonance occurs for a range of τ if the value of c_3 is varied simultaneously.

100-kyr periodicity superimposed on a Lorentzian spectrum. Notably, both spectra also exhibit a high-frequency transition to $f^{-\frac{1}{2}}$ behavior. At the highest frequencies, power in the model spectrum drops as an artifact of the simulation method. Specifically, the viscoelastic load was averaged at timescales less than 1 kyr to speed up the code for long runs.

[37] Histograms of the Vostok and model data are plotted in Figures 9a and 9b, respectively. Histograms of 1000 model samples have been averaged to obtain Figure 9b. Both histograms are bimodal, reflecting the stable states of the system. The asymmetry of the model and observed data are reflected in the larger peak near the full glacial climate.

[38] I have also performed sensitivity studies to determine the variations in model behavior with each of the model parameters. Figure 10 illustrates the effects of varying the Maxwell relaxation time, τ , on the model behavior. Figures 10a, 10b, and 10c correspond to model output with $\tau = 7, 10,$ and 15 kyr, respectively, holding the other model parameters fixed. Resonance is only observed for a narrow range of τ , as illustrated by the very different behaviors obtained with $\tau = 7, 10,$ and 15 kyr. Resonance does not necessarily require a specific value of τ , however, because resonance may be obtained for a range of values of τ by varying both τ and c_3 simultaneously. In other words, if a different value of τ is chosen, such as 5 kyr, the value of the free parameter c_3 can be varied to reestablish coherence resonance. Figure 11a, for example, illustrates the model behavior for $\tau = 20$ kyr and $c_3 = 50$, and Figure 11b

illustrates the model behavior for $\tau = 5$ kyr and $c_3 = 12$. These models yield similar behavior.

[39] The effects of varying the standard deviation of the noise term, c_4 , are illustrated in Figures 12a, 12b, and 12c

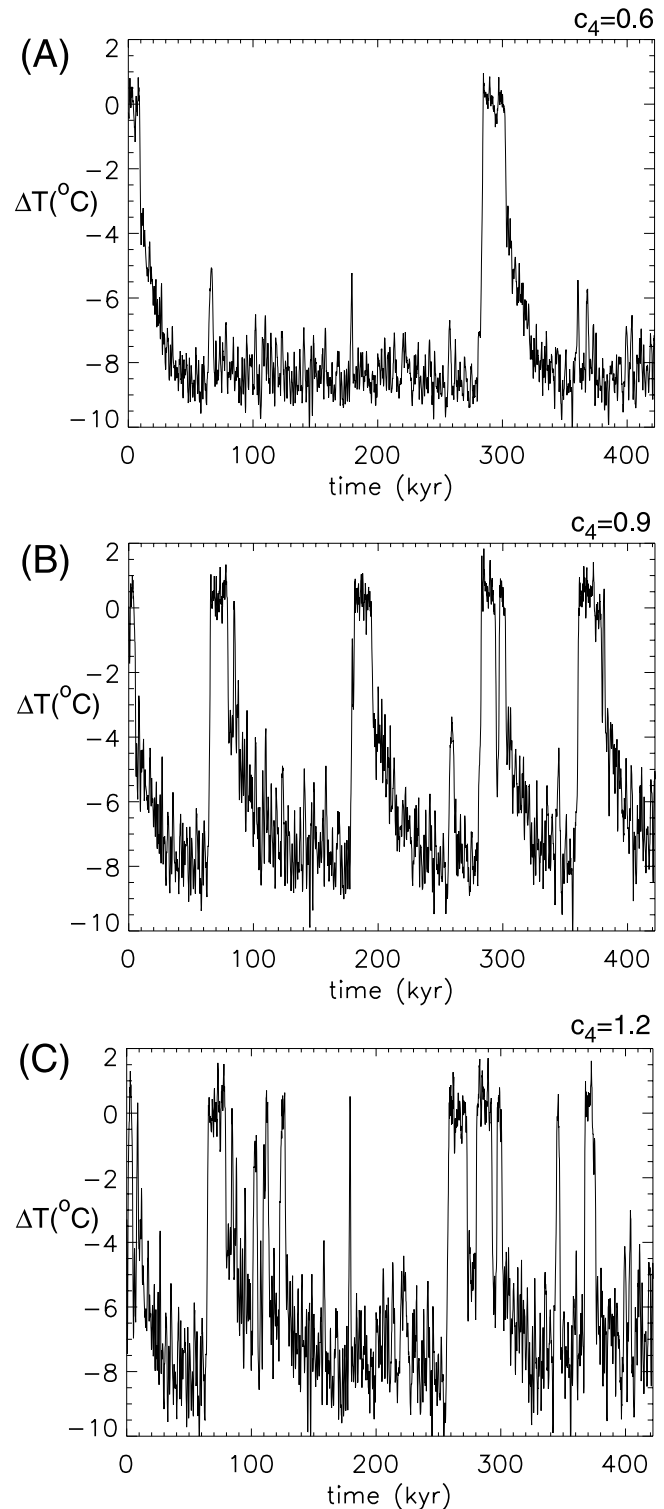


Figure 12. Effects of varying the variance of the noise term, c_4 , on model behavior. (a) $c_4 = 0.6$, (b) $c_4 = 0.9$, and (c) $c_4 = 1.2$. Smaller values of c_4 yield less periodic behavior and fewer transitions. Larger values yield more frequent transitions with less periodic behavior.

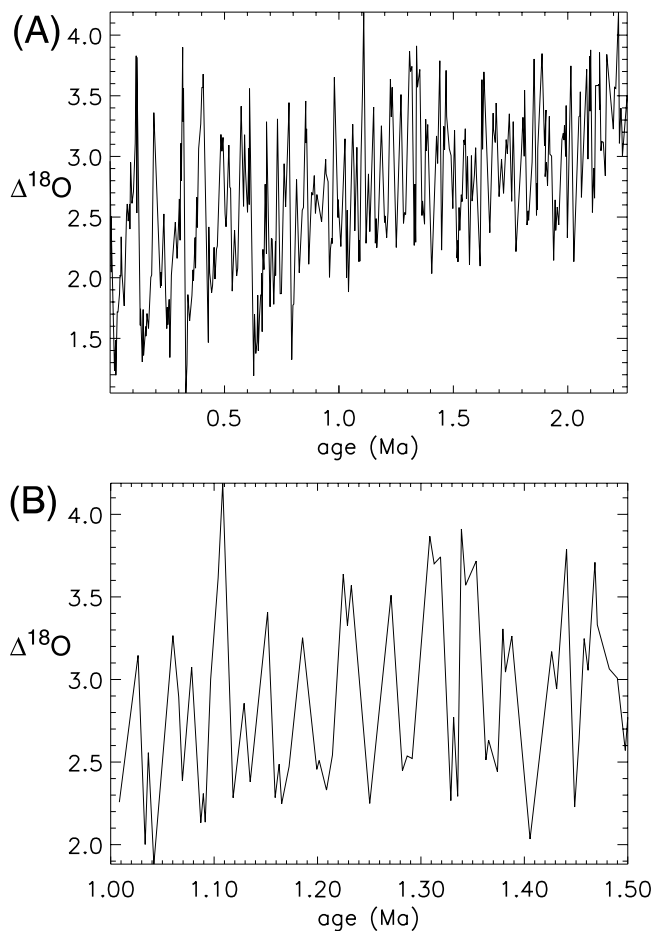


Figure 13. Mid-Pleistocene transition: (a) Benthic $\delta^{18}O$ record from DSDP core 607 illustrating the Mid-Pleistocene transition from small-amplitude 40-kyr cycles to larger-amplitude 100-kyr cycles. (b) Early Pleistocene (1–1.5 Ma) portion of the time series in Figure 13a.

for $c_4 = 0.6, 0.9,$ and $1.2,$ respectively. A smaller value for c_4 results in less-frequent transitions and less-periodic behavior than for the reference case of $c_4 = 0.9.$ An increase in c_4 yields less periodic behavior and more frequent transitions. These results indicate that coherence resonance would not occur if the short-term temperature variations of the climate system were very different from about $1^\circ C$ every 200 years.

5. Mid-Pleistocene Transition

[40] So far I have focused on the Late Pleistocene record of 100-kyr cycles. However, an equally important question is why these cycles did not occur in the Early Pleistocene or before that time. Paleoclimatic proxies that span the Late Pleistocene record a transition from small-amplitude 40-kyr cycles to large-amplitude 100-kyr cycles near 800 ka. These cycles are superimposed on a gradual cooling trend. As an example, the benthic $\delta^{18}O$ record from DSDP 607 is plotted in Figure 13a in the usual way, with increasing age toward the right. This time series is representative of paleoclimatic proxies that span 1 Myr [Raymo, 1994]. The Early Pleisto-

cene climate record, illustrated by the 1–1.5 Ma interval of the DSDP 607 core (shown in Figure 13b) is characterized by 40-kyr cycles. Figure 13a illustrates that the mean temperature of the Early Pleistocene was warmer and the temperature range was smaller than those in the Late Pleistocene. An additional difference between the 40-kyr cycles of the Early Pleistocene and the 100-kyr cycles of the Late Pleistocene is the variability in the maximum and minimum temperatures between cycles. While high (interglacial) and low (glacial) temperatures of the Late Pleistocene were consistent from cycle to cycle, the highs and lows of the Early Pleistocene were significantly more variable.

[41] The model I have presented suggests a simple interpretation of the transition from Early Pleistocene to Late Pleistocene behavior illustrated in Figure 14b. If temperatures in the Early Pleistocene were too high to initiate continental ice sheet growth, the dominant process in the climate system would have been limited to the negative feedback mechanism of long-wavelength outgoing radiation. In this case, the climate-model equation would be characterized by only two terms: temperature-dependent

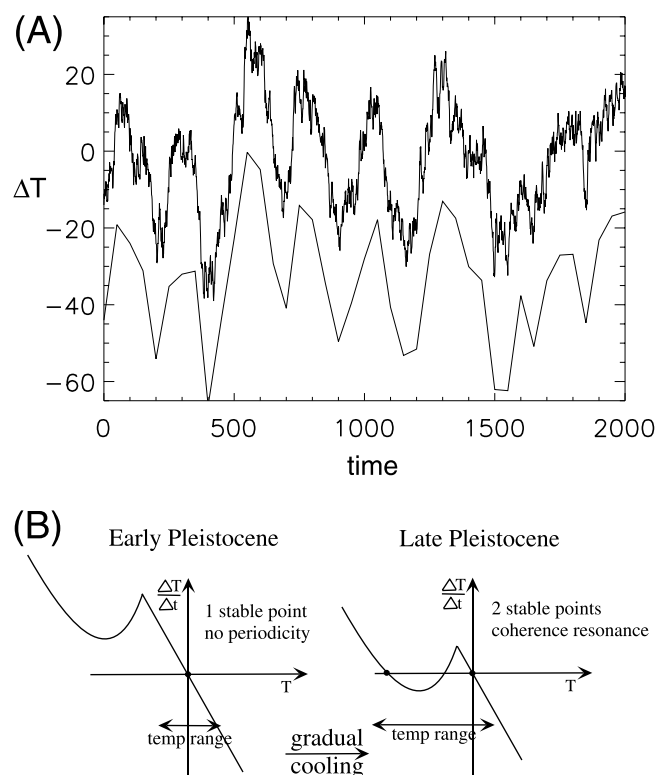


Figure 14. (a) Time series output of equation (2) illustrating an apparent periodicity even though none is present in the underlying dynamics. When such a series is tuned to 41 kyr, the series would appear even more periodic. (b) Schematic diagram of proposed radiation balance in the Early versus Late Pleistocene. In the Early Pleistocene the climate system is too warm to initiate extensive, low-elevation ice sheets and the system fluctuates around a single fixed point. In the Late Pleistocene, however, gradual cooling has shifted the system into larger-amplitude fluctuations with a 100-kyr cycle and two fixed points.

outgoing radiation and random variability, or equation (4). Equation (4) describes a climate system with only one fixed point equal to the mean temperature of the Early Pleistocene. This model produces a time series with a Lorentzian power spectrum. Equation (4) does not have cyclic behavior. The evidence for cyclic behavior in the Early Pleistocene should be examined cautiously, however, because the DSDP 607 time series was tuned to the obliquity period of 41 kyr. Tuning is problematic because it may introduce significant peaks where none exist. P. Huybers (Milankovitch and tuning, unpublished manuscript available online at <http://www.mit.edu/phuybers/General/index.html>, 2001), for example, has illustrated the effects of tuning on white noise. He showed that periodicities comparable in significance to the 41 and 29 kyr peaks attributed to orbital forcing could be obtained by tuning white noise in the way that DSDP cores are tuned. His analysis implies that tuning cannot be used to infer the strength of periodicities at the tuning frequency (other frequencies are less tainted).

[42] Time series produced with equation (4) may appear to be cyclic even when there is no cyclicity present. The apparent cyclicity would occur at the “bend” in the Lorentzian spectrum, where higher frequencies are strongly damped. For example, consider the output time series of equation (4) given in Figure 14a. Two versions of the time series have been presented: the complete time series (top) and a version subsampled close to the frequency at the bend of the spectrum (bottom). Both time series appear to have a weak cyclicity with a period approximately equal to 200 time steps. However, an important clue to the aperiodic nature of this time series is the variability in the highs and lows between “cycles.” This variability reflects significant spectral power at low frequencies, reflecting that fact that the power spectrum of this process has a bend in the spectrum rather than a peak. This demonstration suggests that Early Pleistocene climate may be more accurately described by a Lorentzian spectrum than a periodic spectrum. It is difficult, however, to be certain without more reliable age control.

[43] This proposed interpretation of the Early Pleistocene climate system is consistent with the large variability in highs and lows that characterize Early Pleistocene climate variability. This interpretation suggests that the system is not switching between two stable states but is fluctuating about a single stable state. In addition, the higher mean temperature and smaller temperature range that characterize the Early Pleistocene are consistent with this interpretation. The transition from Early to Late Pleistocene variability in this model may be understood as a threshold transition from a system with one fixed point to a system with two fixed points, brought about by gradual cooling.

6. Conclusions

[44] Climate research has evolved toward the recognition of an increasingly broad array of potentially important factors and more complex models. While this trend has led to a more mature understanding of the of the climate system, it has not led to better agreement on which processes responsible for many of the features of Pleisto-

cene-climate variability, including the dominant 100-kyr cycle.

[45] I have attempted to clarify the issues and focus the debate on the origin of the 100-kyr periodicity on processes that may be reliably constrained. The results suggest that long-wavelength outgoing radiation, the ice-albedo feedback, and lithospheric deflection control the principle features of Pleistocene climate through the simple process of coherence resonance. It should be emphasized that many aspects of the Pleistocene climate system are not included in the model, including Dansgaard-Oeschger events and many other important phenomena in Pleistocene climate. As such, the simple model I propose should not be taken as a full description of the climate system. Nevertheless, the model of this paper is well constrained and matches many important aspects of global climate on timescales of 10^3 – 10^6 years with only one free parameter.

[46] **Acknowledgments.** I thank two anonymous reviewers for their helpful comments. This work was partially supported by NSF EAR-0309518.

References

- Bender, M., T. Sowers, M.-L. Dickson, J. Orchardo, P. Grootes, P. A. Mayewski, and D. A. Meese, Climate correlations between Greenland and Antarctica during the past 100,000 years, *Nature*, 372, 663–666, 1994.
- DeBlonde, G., and W. R. Peltier, Late Pleistocene ice age scenarios based on observational evidence, *J. Clim.*, 6, 709–727, 1993.
- Ganopolski, A., and S. Rahmsdorf, Rapid changes of glacial climate simulated in a coupled climate model, *Nature*, 409, 153–158, 2001.
- Giacomelli, G., M. Giudici, S. Balle, and J. R. Tredicce, Experimental evidence of coherence resonance in an optical system, *Phys. Rev. Lett.*, 84, 3298–3301, 2000.
- Hasselmann, K., Stochastic climate modeling, Part I: Theory, *Tellus*, 6, 473–485, 1971.
- Hyde, W. T., and W. R. Peltier, Sensitivity experiments with a model of the Ice Age: The response to harmonic forcing, *J. Atmos. Sci.*, 42, 2170–2188, 1985.
- Imbrie, J., and J. Z. Imbrie, Modeling the climatic response to orbital variations, *Science*, 207, 943–953, 1980.
- Komintz, M., and N. G. Piasis, Pleistocene climate: Deterministic or stochastic?, *Science*, 204, 171–172, 1979.
- Lee, S. G., A. Neiman, and S. Kim, Coherence resonance in a Hodgkin-Huxley neuron, *Phys. Rev. E*, 57, 3292–3297, 1998.
- LeTreut, H., and M. Ghil, Orbital forcing, climatic interactions, and glaciation cycles, *J. Geophys. Res.*, 88, 5167–5190, 1983.
- Liu, Z. H., Y. C. Lai, and J. M. Lopez, Noise-induced enhancement of chemical reactions in nonlinear flows, *Chaos*, 12, 417–425, 2002.
- Masoller, C., Noise-induced resonance in delayed feedback systems, *Phys. Rev. Lett.*, 88, 034102, 2002.
- Matteucci, G., Orbital forcing in a stochastic resonance model of the Late-Pleistocene climatic variations, *Clim. Dyn.*, 3, 179–190, 1989.
- Matteucci, G., Analysis of the probability distribution of the Late Pleistocene climatic record: Implications for model validation, *Clim. Dyn.*, 5, 35–52, 1990.
- Nicolis, C., and G. Nicolis, Is there a climatic attractor?, *Nature*, 311, 529–532, 1984.
- North, G., *Paleoclimatology*, Oxford Univ. Press, New York, 1991.
- North, G., R. Cahalan, and R. Moeng, Energy balance climate models, *Rev. Geophys.*, 19, 90–121, 1981.
- Nye, J. F., The flow of glaciers and ice sheets as a problem in plasticity, *Proc. R. Soc. London, Ser. A*, 207, 554–572, 1951.
- Oerlemans, J., Continental ice sheets and the planetary radiation budget, *Quat. Res.*, 14, 349–359, 1980a.
- Oerlemans, J., Model experiments on the 100,000 year glacial cycle, *Nature*, 287, 430–432, 1980b.
- Paillard, D., The timing of Pleistocene glaciations from a simple multiple-state climate model, *Nature*, 391, 378–381, 1998.
- Pelletier, J. D., Analysis and modeling of the natural variability of climate, *J. Clim.*, 10, 1331–1342, 1997.
- Peltier, W. R., Ice Age paleotopography, *Science*, 265, 195–201, 1994.
- Petit, J. R., et al., Climate and atmospheric history of the past 420,000 years from the Vostok ice core, Antarctica, *Nature*, 399, 429–436, 1999.

- Pikovsky, A. S., and J. Kurths, Coherence resonance in a noise-driven excitable system, *Phys. Rev. Lett.*, 78, 775–778, 1997.
- Pollard, D., A coupled climate-ice sheet model applied to the Quaternary ice ages, *J. Geophys. Res.*, 88, 7705–7718, 1983.
- Press, W. H., S. A. Teukolsky, W. T. Vetterling, and B. P. Flannery, *Numerical Recipes in C: The Art of Scientific Computing*, 2nd ed., Cambridge Univ. Press, New York, 1992.
- Raymo, M., The initiation of Northern Hemisphere glaciation, *Annu. Rev. Earth Planet. Sci.*, 22, 353–383, 1994.
- Raymo, M., Glacial puzzles, *Science*, 281, 1467–1468, 1998.
- Saltzman, B., and A. Sutera, A model of the internal feedback system involved in Late Quaternary climatic variations, *J. Atmos. Sci.*, 41, 736–745, 1984.
- Short, D. A., G. R. North, T. D. Bess, and G. L. Smith, Infrared parameterization and simple climate models, *J. Clim. Appl. Meteorol.*, 23, 1222–1233, 1984.
- Tarasov, L., and W. R. Peltier, Impact of thermomechanical ice sheet coupling on a model of the 100 kyr ice age cycle, *J. Geophys. Res.*, 104, 9517–9545, 1999.
- Tsimring, L. S., and A. Pikovsky, Noise-induced dynamics in bistable systems with delay, *Phys. Rev. Lett.*, 87, 250602, 2001.
- Tziperman, E., and H. Gildor, On the mid-Pleistocene transition to 100-kyr glacial cycles and the asymmetry between glaciation and deglaciation times, *Paleoceanography*, 18(1), 1001, doi:10.1029/2001PA000627, 2003.
- van der Sluijs, J. P., G. J. de Bruyn, and P. Westbroek, Biogenic feedbacks in the carbonate-silicate geochemical cycle and the global climate, *Am. J. Sci.*, 296, 932–953, 1996.
- van Kampen, N. G., *Stochastic Processes in Physics and Chemistry*, North-Holland, New York, 2001.
- Watts, A. B., *Isostasy and Flexure of the Lithosphere*, Cambridge Univ. Press, New York, 2001.

J. D. Pelletier, Department of Geosciences, University of Arizona, Gould-Simpson Building, 1040 E. Fourth Street, Tucson, AZ 85721-0077, USA. (jon@geo.arizona.edu)